# Optimal Displacement Sensing with Spin-Dependent Squeezed States

Liam J. Bond,[1,2,*] Christophe H. Valahu,[3,4] Athreya Shankar,[5,6] Ting Rei Tan,[3,4] and Arghavan Safavi-Naini[1,2]

[1] Institute of Physics, University of Amsterdam, Science Park 904, 1098 XH Amsterdam, the Netherlands
[2] QuSoft, Science Park 123, 1098 XG Amsterdam, the Netherlands
[3] School of Physics, University of Sydney, NSW 2006, Australia
[4] Sydney Nano Institute, University of Sydney, NSW 2006, Australia
[5] Department of Physics, Indian Institute of Technology Madras, Chennai 600036, India
[6] Center for Quantum Information, Communication and Computing, Indian Institute of Technology Madras, Chennai 600036, India

(Received 17 November 2025; revised 17 March 2026; accepted 28 April 2026; published 23 June 2026)

Displacement sensing is a fundamental task in metrology. However, the development of quantum-enhanced sensors that fully utilize the available degrees of freedom in many-body quantum systems remains an outstanding challenge. We propose many-body displacement sensing schemes that use spin-dependent squeezed (SDS) states—hybrid spin-boson states whose bosonic squeezed quadrature is conditioned on an auxiliary spin. We prove that SDS states are *optimal*, i.e., their quantum Cramér-Rao bound saturates the Heisenberg limit. We propose explicit measurement sequences that can be readily implemented in systems such as trapped ions. We also introduce a scalable state-preparation protocol and numerically demonstrate the preparation of 8.7 dB of spin-dependent squeezing 15 times faster than the standard approach using second-order sidebands in trapped ions. The potential applications of our sensing protocols range from measuring single-photon scattering to searches for dark matter.

DOI: 10.1103/mhvv-pr5d

## I. INTRODUCTION

Measuring the response of a system to estimate an unknown parameter underpins the development of science and technology. For example, the detection of gravitational waves at the Laser Interferometer Gravitational-Wave Observatory (LIGO) confirmed one of the most important predictions of the general theory of relativity [1,2], while precision spectroscopy in atomic clocks has revolutionized timekeeping with fractional uncertainties now below $10^{-18}$ [3,4]. At the same time, significant efforts have been devoted to using quantum systems for sensing theorized couplings between Standard Model fields and dark-matter candidates such as dark photons, millicharged dark matter or axions [5–7]. Such couplings would induce ultrasmall bosonic *displacements* of a microwave field [7–11] or a mechanical oscillator [6,12–16], which could be measured by a sufficiently sensitive displacement sensor.

The sensitivity of the quantum sensor crucially depends on its initial reference state. Using a classical, uncorrelated reference state, the estimation variance is lower bounded by the so-called standard quantum limit (SQL). For displacement sensing, the SQL is defined by bosonic coherent states and is constant, SQL $\propto \mathcal{O}(1)$. As such, the sensitivity cannot be improved by simply increasing the amplitude of the coherent state. By instead using nonclassical reference states and quantum measurement protocols, the estimation variance is ultimately limited by Heisenberg scaling, HS $\propto 1/\langle\hat{n}\rangle$, where $\langle\hat{n}\rangle$ is the reference state's average bosonic occupation [17]. This is known as *quantum-enhanced sensing*.

Previous works have considered a range of different bosonic reference states for quantum-enhanced displacement sensing. Examples of states that can achieve sub-SQL sensitivities are Fock states [18,19] and their (optimal) superpositions [20], phase-twirled squeezed states [21] and two- and four-component cat states [7,22]. Simultaneous sub-SQL sensing of a displacement's real and imaginary phase-space component can also be achieved using, for example, single-mode grid states [23–25] and two-mode squeezed states [26–28].

*Contact author: L.J.Bond@uva.nl

*Published by the American Physical Society under the terms of the Creative Commons Attribution 4.0 International license. Further distribution of this work must maintain attribution to the author(s) and the published article's title, journal citation, and DOI.*

However, the aforementioned reference states do not take full advantage of the available degrees of freedom in *many-body* experimental platforms, which feature exquisite control over both spin and bosonic degrees of freedom [29–33]. Such many-body systems are ideal quantum sensors as they offer the possibility of *collective enhancement* for faster reference state preparation, or for amplification of the displacement signal. For example, spin-boson cat states are prepared $\sqrt{N}$ times faster in a trapped-ion system with $N$ ions, while electric field sensing benefits from a $\sqrt{N}$ amplification of the displacement signal when using $N$ ions [15]. While there are existing protocols for single-parameter displacement sensing in many-body systems [15,34,35], there is a lack of sensing protocols that utilize the advantages of many-body quantum systems for estimating a displacement's amplitude, or jointly estimating its real and imaginary components.

Here, we solve this problem by introducing many-body displacement sensing schemes using spin-dependent bosonic squeezed states—hybrid spin-boson states whose bosonic squeezed quadrature is conditioned on the state of an auxiliary spin. We prove that such states are *optimal* reference states for both amplitude and joint-parameter displacement sensing, with quantum Cramér-Rao bounds (QCRBs) that saturate the Heisenberg limit. We develop explicit measurement protocols that follow Heisenberg scaling and can be readily implemented on existing quantum hardware platforms. We propose a scalable protocol for preparing spin-dependent squeezed (SDS) states in trapped ions that requires only global addressing, and numerically demonstrate that for $N = 20$ ions our protocol achieves 8.7 dB of spin-dependent squeezing 15 times faster than the usual approach of driving the second-order sidebands. Our state-preparation protocol also has immediate applications to quantum computing with both discrete [36–38] and continuous [39,40] variable systems. Finally, we prove that the metrological utility of SDS states is insensitive to single-spin dephasing, and from numerics observe robustness to motional dephasing and heating. Although our explicit measurement protocols are less robust, when taking into account the collective enhancements that are available in trapped ions, we identify parameter regimes where the metrological utility of our protocols increases with the number of ions, realizing a collective enhancement.

## II. DISPLACEMENT SENSING

Consider a system of $N$ spins and a single bosonic mode, prepared in a reference state, $|\psi_{\text{ref}}\rangle$. The reference state is subjected to a small, coherent displacement by an unknown amount $\beta \in \mathbb{C}$, described by the displacement operator, $\hat{D}(\beta) = \exp\left(\beta\hat{a}^\dagger - \beta^*\hat{a}\right)$. The resulting displaced state is

$$|\psi(\boldsymbol{\theta})\rangle = \hat{D}(\beta)\,|\psi_{\text{ref}}\rangle\,, \tag{1}$$

which encodes a set of $d$ real parameters, $\boldsymbol{\theta} = \{\theta_1, \theta_2, \ldots, \theta_d\}$. Here, $\boldsymbol{\theta}$ is related to $\beta$. We review quantum multiparameter metrology in more detail in the Supplemental Material [41].

Our goal is to estimate $\boldsymbol{\theta}$ from a set of $M$ independent measurement outcomes, $\boldsymbol{x} = \{x_1, \ldots, x_M\}$. The uncertainty of the estimation is quantified by the covariance matrix, $\boldsymbol{V}(\boldsymbol{\theta}) = \sum_{\boldsymbol{x}} p(\boldsymbol{x}|\boldsymbol{\theta})[\boldsymbol{\theta} - \tilde{\boldsymbol{\theta}}(\boldsymbol{x})][\boldsymbol{\theta} - \tilde{\boldsymbol{\theta}}(\boldsymbol{x})]^T$, where $p(\boldsymbol{x}|\boldsymbol{\theta})$ are the measurement probabilities and $\tilde{\boldsymbol{\theta}}(\boldsymbol{x})$ an unbiased estimator.

For a chosen reference state and measurement observable, minimizing over all possible unbiased estimators lower bounds $\boldsymbol{V}$ according to the classical Cramér-Rao bound (CCRB),

$$\text{Tr}(\boldsymbol{V}) \geq \text{Tr}(\boldsymbol{F}^{-1}), \tag{2}$$

where we set $M = 1$ and where the classical Fisher information matrix $\boldsymbol{F}$ is

$$F_{ij} = \sum_k \frac{1}{p(x_k|\boldsymbol{\theta})}[\partial_i p(x_k|\boldsymbol{\theta})][\partial_j p(x_k|\boldsymbol{\theta})], \tag{3}$$

with $\partial_i = \partial/\partial\theta_i$. Further optimizing over all possible measurement observables, $\boldsymbol{V}$ is lower bounded by the QCRB [42,43],

$$\text{Tr}(\boldsymbol{V}) \geq \text{Tr}(\boldsymbol{Q}^{-1}), \tag{4}$$

where the quantum Fisher information (QFI) matrix $\boldsymbol{Q}$ is

$$Q_{ij} = \frac{1}{2}\,\langle\psi(\boldsymbol{\theta})|\,\{\hat{L}_i, \hat{L}_j\}\,|\psi(\boldsymbol{\theta})\rangle\,, \tag{5}$$

with $\hat{L}_i$ the symmetric logarithmic derivative [41]. In general, finding explicit measurement observables whose classical Fisher information matrix saturates the QFI matrix is a nontrivial task.

Typically, displacement sensing is performed in the paradigm of metrology by repetition, in which a single experimental shot—consisting of reference state preparation, linear interaction with the signal, and measurement—is repeated many times. It is therefore important to establish whether the relative phase between the reference state and the unknown displacement varies between experimental shots. This leads to two settings:

(i) *Phase-insensitive sensing of the displacement's magnitude*: If the phase varies between experimental shots, we can only estimate the displacement magnitude, so $\boldsymbol{\theta} = |\beta|$.

(ii) *Single- or multiparameter sensing*: If the phase is fixed between shots, we can decompose $\beta = \beta_{\text{re}} + i\beta_{\text{im}}$. We can estimate a single parameter, so

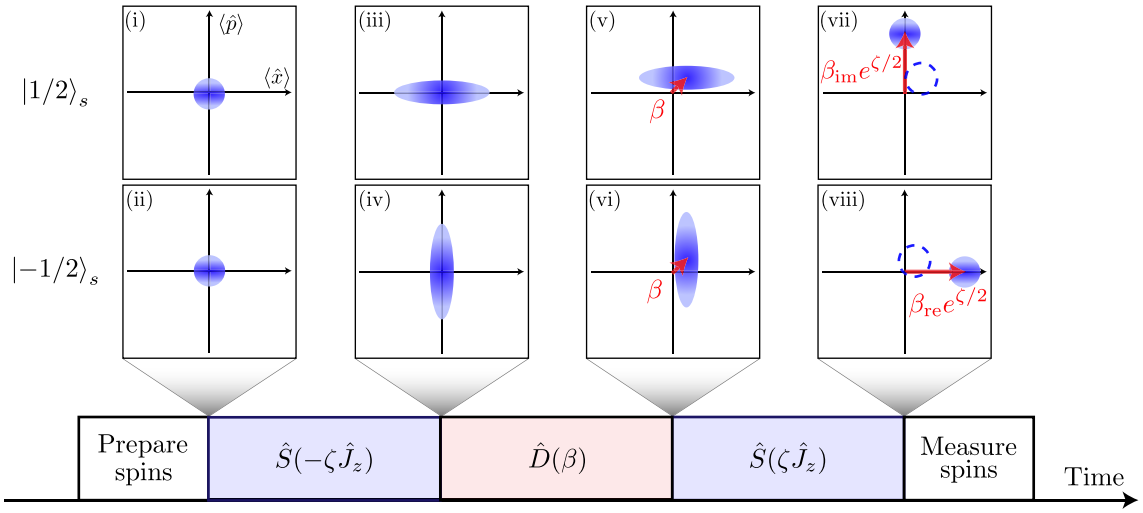



FIG. 1. Protocol steps for phase-insensitive sensing of a displacement amplitude using spin-dependent squeezed states. Top (bottom) row shows for $N = 1$ spin, schematic representations of the bosonic Wigner function associated with the spin $|1/2\rangle_s$ ($|-1/2\rangle_s$) state. After initialization to $|0\rangle_b|\psi_0\rangle_s \cong |0\rangle_b(|-1/2\rangle_s + |1/2\rangle_s)$, [panels (i) and (ii)], spin-dependent squeezing $\hat{S}(-\zeta\hat{J}_z)$ squeezes the bosonic mode conditioned on the spin state [panels (iii) and (iv)]. The bosonic mode then undergoes an unknown displacement $\hat{D}(\beta)$ [panels (v) and (vi)]. Finally, the spin-dependent squeezing is reversed [panels (vii) and (viii)]. The signal's imaginary part, $\beta_{\rm im}$, is exponentially amplified in the $|1/2\rangle_s$ Hilbert space sector, while the real part, $\beta_{\rm re}$, is amplified in the $|-1/2\rangle_s$ sector. Unlike the phase-insensitive amplification protocol of Ref. [44], here the signal amplification is spin-dependent. Phase-insensitive information about the displacement is accessed via a spin measurement. Without spin-dependent squeezing, the final state is a purely bosonic displaced state (blue dashed circles).

$\boldsymbol{\theta} = \{\beta_{\rm re}\}$ or $\boldsymbol{\theta} = \{\beta_{\rm im}\}$, or jointly estimate both parameters, so $\boldsymbol{\theta} = \{\beta_{\rm re}, \beta_{\rm im}\}$.

Minimizing the QCRB over all possible reference states yields the Heisenberg limit (HL). Here, we take the minimization to be over all possible single-mode bosonic reference states, see the Supplemental Material [41]. In terms of the reference state's average mode occupation $\langle\hat{n}\rangle$, for single-parameter displacement sensing HL $= 1/(16\langle\hat{n}\rangle + 4)$, for phase-insensitive amplitude sensing HL $= 1/(8\langle\hat{n}\rangle + 4)$ and for multiparameter displacement sensing HL $= 1/(4\langle\hat{n}\rangle + 2)$. If a metrology protocol's CCRB or QCRB equals the HL lower bound, we say that it "saturates the Heisenberg limit", and is therefore "optimal." If it falls inversely with $\langle\hat{n}\rangle$ but with a larger constant prefactor than that of the HL, we say that it "follows Heisenberg scaling."

### A. SDS states

In this work, we consider reference states of the form

$$|\psi_{\rm ref}\rangle = \hat{U}|0\rangle_b|\psi_0\rangle_s. \tag{6}$$

Here, $|0\rangle_b$ is the bosonic vacuum, and $|\psi_0\rangle_s = \sum_{m=-N/2}^{N/2} c_m|m\rangle_s$ is a collective spin state written with coefficients $c_m \in \mathbb{C}$ in the basis of Dicke states, $\hat{J}_z|m\rangle_s = m|m\rangle_s$, where the magnetization $m$ is (half-)integer $-N/2 \le m \le N/2$, and where the collective spin operators are $\hat{J}_\alpha = \sum_{i=1}^N \hat{\sigma}_i^\alpha/2$ with $\alpha = x, y, z$. The unitary $\hat{U}$ entangles the spin and bosonic degrees of freedom; possible choices that have been previously studied include spin-dependent displacements [7,15] or dispersive spin-boson interactions [34,35].

We ask, for each of the metrology settings defined above, what is the optimal reference state? In Fig. 1(a) we sketch the Wigner function for one such state, which is generated by spin-dependent squeezing [36,45],

$$\hat{S}(\zeta\hat{J}_z) = \exp\left(\frac{1}{2}(\zeta^*\hat{a}^2 - \zeta\hat{a}^{\dagger 2})\hat{J}_z\right), \tag{7}$$

where $\zeta$ is the squeezing parameter. The creation and annihilation operators, $\hat{a}^\dagger$ and $\hat{a}$, are related to position and momentum operators via $\hat{x} = \hat{a}^\dagger + \hat{a}$ and $\hat{p} = i(\hat{a}^\dagger - \hat{a})$, respectively. Spin-dependent squeezing is also known as conditional squeeze [39,46,47] or control-squeeze [48,49]. In Sec. III we show how it can be implemented in a fast, scalable manner in trapped-ion systems. We write the reference state obtained from spin-dependent squeezing as

$$|\psi_{\rm ref}\rangle = \hat{S}(\zeta\hat{J}_z)|0\rangle_b|\psi_0\rangle_s = \sum_{m=-N/2}^{N/2} c_m|\zeta m\rangle_b|m\rangle_s, \tag{8}$$

where the bosonic squeezed state is defined as

$$|\zeta m\rangle_b = \hat{S}(\zeta m)|0\rangle_b = e^{\zeta m(\hat{a}^2 - \hat{a}^{\dagger 2})/2}|0\rangle_b. \tag{9}$$

Without loss of generality we set $\zeta \in \mathbb{R}$, which is equivalent to setting the initial phase-space axis.

For $|\psi_0\rangle_s$, we focus on two particular choices: the Greenberger-Horne-Zeilinger (GHZ) state [50] and a spin coherent state (SC) pointing along $x$ of the collective Bloch sphere,

$$|\psi_{\mathrm{GHZ}}\rangle_s = \frac{1}{\sqrt{2}}(|-N/2\rangle_s + |N/2\rangle_s), \tag{10a}$$

$$|\psi_{\mathrm{SC}}\rangle_s = e^{i\pi/2\hat{J}_y}\,|-N/2\rangle_s = \sum_{m=-N/2}^{N/2} c_m\,|m\rangle_s\,, \tag{10b}$$

where $c_m = 2^{-N/2}\sqrt{\binom{N}{m+N/2}}$ for the spin coherent state. It is instructive to visualize the reference states generated by spin-dependent squeezing from each of these initial collective spin states. For $N = 1$ spin, both spin states are the same. In Fig. 1(a) we separately plot the Wigner functions for the $m = 1/2$ (top row) and $m = -1/2$ (bottom row) Hilbert space sectors. The bosonic state is squeezed along orthogonal directions [panels (iii) and (iv)], which indicates utility for phase-insensitive sensing of a displacement amplitude.

### B. Phase-insensitive displacement sensing

We begin in the setting where the phase between displacement and reference state varies between shots, which limits us to sensing the magnitude, $|\beta|$. The metrological utility is quantified by the QFI, cf. the QCRB of Eq. (4).

We consider any initial collective spin state with symmetric Dicke weights, i.e., $|c_m| = |c_{-m}|$. As we derive in the Supplemental Material [41], the QFI is completely independent of $\beta$,

$$\mathcal{Q}_{|\beta|} = 8\sum_{m>0}^{N/2} |c_m|^2 \cosh(2\zeta m), \tag{11}$$

and grows exponentially with squeezing $\zeta$, indicating metrological utility. The corresponding QCRB is

$$V(|\beta|) = \frac{1}{\mathcal{Q}_{|\beta|}} \geq \frac{1}{8\langle\hat{n}\rangle + 4}, \tag{12}$$

where $\langle\hat{n}\rangle = \langle\psi_{\mathrm{ref}}|\hat{n}|\psi_{\mathrm{ref}}\rangle$. The Heisenberg limit for the estimation of $|\beta|$ is $1/(8\langle\hat{n}\rangle + 4)$ [41], and therefore the QCRB saturates the Heisenberg limit. As such, as a function of the available resources (i.e., the mode occupation), the reference state is optimal for phase-insensitive estimation of the displacement's amplitude $|\beta|$.

#### *1. Measurement protocol*

Because the displaced reference state is spin-boson entangled, the metrological advantage is in a mixed spin-boson quadrature, which is often challenging to measure experimentally. This problem is solved by mapping the information to the spin degree of freedom using a time-reversal sequence, shown in Fig. 1(a). The sequence braids to a displacement that depends exponentially on the spin

$$\hat{S}(\zeta\hat{J}_z)\hat{D}(\beta)\hat{S}(-\zeta\hat{J}_z) = \hat{D}(\hat{\beta}), \tag{13}$$

where $\hat{\beta} = \beta\cosh(\zeta\hat{J}_z) - \beta^*\sinh(\zeta\hat{J}_z)$.

We start by considering the sequence for a single spin initialized in

$$|0\rangle_b\,|\psi_0\rangle_s \simeq |0\rangle_b\,(|-1/2\rangle_s + |1/2\rangle_s). \tag{14}$$

The final state is

$$\left|\psi_f\right\rangle \simeq \hat{D}(\beta_-)|0\rangle_b\,|-1/2\rangle_s + \hat{D}(\beta_+)|0\rangle_b\,|1/2\rangle_s\,, \tag{15}$$

where the spin-dependent displacement amplitudes are $\beta_- = \beta_{\mathrm{re}}\exp(\zeta/2) + i\beta_{\mathrm{im}}\exp(-\zeta/2)$ and $\beta_+ = \beta_{\mathrm{re}}\exp(-\zeta/2) + i\beta_{\mathrm{im}}\exp(\zeta/2)$. The parameter $\beta_{\mathrm{re}}$ is exponentially amplified in the spin down Hilbert space sector, while $\beta_{\mathrm{im}}$ is exponentially amplified in the spin up sector [see panels (vii) and (viii) of Fig. 1(a)]. For small displacements $|\beta| \ll 1$, after a $\pi/2$ spin rotation about $\hat{\sigma}_y$, the probability of measuring $|1/2\rangle_s$ is

$$P_{1/2} = 1 - |\beta|^2\sinh(\zeta/2)^2 + \mathcal{O}(\beta^4), \tag{16}$$

which is phase-insensitive up to third order in $\beta$. In the limit $\beta \to 0$, the classical Fisher information (CFI) is

$$F_{|\beta|} = 4\sinh(\zeta/2)^2 = 4\langle\hat{n}\rangle, \tag{17}$$

and therefore the CCRB is

$$V(|\beta|) \geq \frac{1}{F_{|\beta|}} = \frac{1}{4\langle\hat{n}\rangle}, \tag{18}$$

which follows Heisenberg scaling, $\propto 1/\langle\hat{n}\rangle$.

The metrological performance of our measurement protocol with a single spin is shown in Fig. 2, where we plot the CCRB (blue line) and compare it against the QCRB (black line) of Eq. (12). The CCRB diverges from the QCRB as $\langle\hat{n}\rangle \to 0$ because no information is mapped to the spin. For $\langle\hat{n}\rangle \gtrsim 1$, the CCRB follows QCRB scaling but remains a factor of two larger than the Heisenberg limit. When $\langle\hat{n}\rangle \gtrsim 1$ the CCRB falls below the SQL, which is defined by the use of bosonic coherent states as reference states, SQL $= 1/4$ [41].

We next generalize the measurement protocol to $N$ spins, which can potentially offer a beneficial collective enhancement. We begin with the case of the spins in a GHZ state. We assume that the GHZ state is prepared

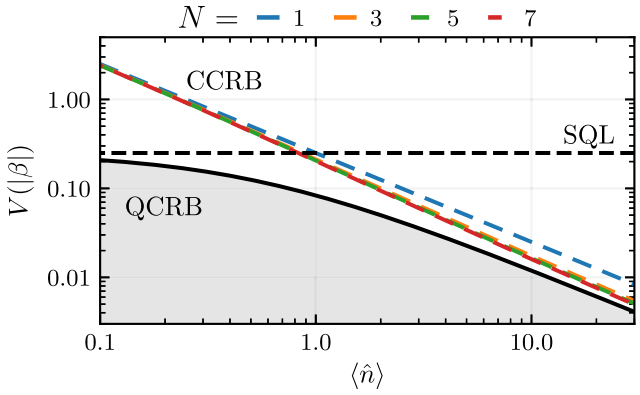



FIG. 2. Metrological performance of spin-dependent squeezed spin coherent states, for phase-insensitive estimation of the displacement's magnitude, $|\beta|$. The classical Cramér-Rao bound for the time-reversal protocol and collective spin measurement (described in the main text) is plotted for increasing numbers of spins, $N$ (solid colored lines). The classical Cramér-Rao bound is below the standard quantum limit (dashed black line) for all $N$ at $\langle\hat{n}\rangle \gtrsim 1$. Moreover, the classical Cramér-Rao bound for $N = 1$ is 10 dB below the standard quantum limit at $\langle\hat{n}\rangle = 10$. The standard quantum limit is defined as the quantum Cramér-Rao bound for bosonic coherent states, which for sensing of $|\beta|$ is SQL $= 1/4$ [41]. The classical Cramér-Rao bound is further compared to the quantum Cramér-Rao bound (solid black line). At $\langle\hat{n}\rangle \gtrsim 1$, the classical Cramér-Rao bound for all $N$ follows Heisenberg scaling, $\propto 1/\langle\hat{n}\rangle$. In this same regime, the classical Cramér-Rao bound for $N = 1$ spin is a factor of two larger than the quantum Cramér-Rao bound. The prefactor decreases to one in the $N \to \infty$ limit.

using a one-axis twisting (OAT) Hamiltonian evolving for time $\pi/2$,

$$\hat{U}_{\mathrm{OAT}} = \exp\left(-\frac{\pi}{2}\hat{J}_x^2\right). \tag{19}$$

For the case of even $N$, after initializing all spins in spin down, evolving under $\hat{U}_{\mathrm{OAT}}$ produces $\hat{U}_{\mathrm{OAT}}\,|-N/2\rangle_s = 1/\sqrt{2}(e^{-i\pi/4}\,|-N/2\rangle + e^{i\pi/4+i\pi N/2}\,|N/2\rangle)$, which is the same form as the GHZ state of Eq. (10a) but with different relative phases. After applying the time-reversal protocol of Eq. (13), we reverse the one-axis twisting and measure in the Dicke basis (see Supplemental Material [41] for details). The only two states with nonzero measurement probabilities are $P_{N/2}$ and $P_{-N/2} = 1 - P_{N/2}$. For small displacements $\beta \ll 1$, they are

$$P_{N/2} = |\beta|^2 \sinh(N\zeta/2)^2 + \mathcal{O}(\beta^4). \tag{20}$$

The corresponding CFI in the limit $\beta \to 0$ is

$$F_{|\beta|} = 4\sinh(N\zeta/2)^2 = 4\langle\hat{n}\rangle. \tag{21}$$

As a function of $\langle\hat{n}\rangle$, this many-spin CFI is identical to the single-spin result of Eq. (18). The advantage of using $N$ spins lies in a potential collective enhancement. For example, in trapped ions there is a $\sqrt{N}$ amplification of the displacement signal, as well as a $\sqrt{N}$ reduction in state-preparation time, as we show later in Sec. III.

Next, we consider $N$ spins initialized in the spin coherent state of Eq. (10b). For small displacements $\beta \ll 1$, after a collective $\pi/2$ spin rotation about $\hat{J}_y$, the probability of measuring each Dicke state is phase-insensitive up to third order in $\beta$ (see Supplemental Material [41] for derivation). The exact CFI is of the form

$$F_{|\beta|} = \sinh(\zeta/2)^2 \sum_{i=0}^{N-1} a_i \cosh(i\zeta), \tag{22}$$

where the coefficients $a_i$ are specified in the Supplemental Material [41]. The metrological performance is shown in Fig. 2, where we plot the CCRB, $1/F_{|\beta|}$, for increasing $N$, as well as the QCRB (black line) of Eq. (12) which is independent of $N$. For $\langle\hat{n}\rangle \approx 1$, the CCRB is a factor of approximately two larger than the QCRB. The CCRB is below the SQL (black dashed line) for $\langle\hat{n}\rangle \gtrsim 1$. Taking the limit $\langle\hat{n}\rangle \to \infty$, the ratio between the CFI and QFI is,

$$\frac{Q_{|\beta|}}{F_{|\beta|}} = \frac{2^N}{2^N - 1}, \tag{23}$$

which approaches one in the limit $N \to \infty$. Therefore, in this extreme regime, the CCRB for phase-insensitive sensing of the displacement's amplitude with SDS spin coherent states saturates the Heisenberg limit [41].

### C. Multiparameter displacement sensing

Next, we consider the setting where the phase is fixed between experimental shots, and perform joint estimation of $\beta_{\mathrm{re}}$ and $\beta_{\mathrm{im}}$. For any symmetric Dicke weights $|c_{-m}| = |c_m|$, we prove in the Supplemental Material [41] that the QFI matrix is

$$\mathbf{Q} = 8\sum_{m>0}^{N/2}\left[|c_m|^2\cosh(2\zeta m)\right]\mathbb{1} = (8\langle\hat{n}\rangle + 4)\mathbb{1}. \tag{24}$$

The corresponding multiparameter QCRB is

$$V(\beta_{\mathrm{re}}) + V(\beta_{\mathrm{im}}) \geq \frac{1}{4\langle\hat{n}\rangle + 2}, \tag{25}$$

which saturates the multiparameter Heisenberg limit, and therefore symmetric Dicke weight SDS states are optimal reference states. In the Supplemental Material [41], we further study the multiparameter QCRB as a function of the squeezing parameter $\zeta$, and show that reference states obtained from GHZ spin states outperform those obtained from sin coherent states, because the mode occupation $\langle\hat{n}\rangle$ as a function of $\zeta$ is higher.

When jointly estimating two or more parameters, the optimal measurement for each parameter may be different, and the set of optimal measurements may be incompatible. If this is the case, the attainable estimation uncertainty is determined by the Holevo-Cramér-Rao bound (HCRB). The HCRB is at most two times larger than the QCRB, $\mathrm{QCRB} \leq \mathrm{HCRB} \leq (1+R)\mathrm{QCRB}$, where $R \in [0,1]$ is the asymptotic incompatibility (see the Supplemental Material [41] and Ref. [51]). For symmetric Dicke weight SDS states, we calculate the asymptotic incompatibility,

$$R = \frac{1}{2\langle \hat{n} \rangle + 1}, \tag{26}$$

and so the HCRB approaches the QCRB in the infinite squeezing limit because $R \to 0$ when $\langle \hat{n} \rangle \to \infty$.

### *1. Measurement protocol*

Similar to the phase-insensitive setting, accessing the metrological advantage of the mixed spin-boson quadrature to perform multiparameter displacement sensing is challenging. Here, we provide one possible measurement protocol that uses two ancilla qubits. As shown in Fig. 3(a), the sequence is built by wrapping the time-reversal sequence in spin-dependent displacements of strength $g$ that are conditioned on the state of each ancilla. Each ancilla is then measured simultaneously and independently in the Dicke basis.

Our analysis focuses on the single spin case. When the spin-dependent squeezing is much larger than both the spin-dependent displacement, $\zeta \gg g$, and the displacement signal, $\zeta \gg \beta$, information about the displacement's real component is mapped only to the first ancilla, while information about the imaginary component is mapped only to the second ancilla. The probability of measuring the $i$th ancilla in the $|+\rangle$ state is then (see Supplemental Material [41]),

$$P_+^{(i)} = \frac{1}{2}[1 + \cos^2(\phi_i)], \tag{27}$$

where $\phi_1 = 2g\exp(\zeta)\beta_{\mathrm{re}}$, and $\phi_2 = -2g\exp(\zeta)\beta_{\mathrm{im}}$. In the limit $\beta \to 0$, the CFI matrix is $\mathbf{F} = 8g^2e^{2\zeta}\mathbb{1}$. The multiparameter variance is therefore lower bounded by the CCRB according to

$$V(\beta_{\mathrm{re}}) + V(\beta_{\mathrm{im}}) \geq \frac{1}{4g^2e^{2\zeta}}. \tag{28}$$

In Fig. 3(b), we show for various $g$ the CCRB obtained from the approximate analytic expression of Eq. (28) (dotted lines) and from numerical simulations of the measurement sequence (solid colored dots). Due to the additional spin-dependent displacements in the time-reversal protocol, the reference state, i.e., the state before exposure to the signal, becomes $|\psi_{\mathrm{ref}}\rangle = \hat{S}(-\zeta\hat{J}_z)\hat{D}(-ig\hat{\sigma}_z^{(1)})\hat{D}(-g\hat{\sigma}_z^{(2)})\,|0\rangle_b\,|\psi_0\rangle_s\,|+\rangle_1\,|+\rangle_2$, which is the state used to calculate $\langle \hat{n} \rangle$. For all curves, when $\zeta \gg g$ we observe excellent agreement between theory and numerics. For increasing $g$, the curves are shifted to the right due to the larger $\langle \hat{n} \rangle$. For $\langle \hat{n} \rangle \gtrsim 1$, the CCRBs follow the Heisenberg scaling of the QCRB (black line), with a prefactor that decreases with increasing $g$. At $g = 0.4$, the estimation uncertainty is below the SQL (black dashed line) when $\langle \hat{n} \rangle \gtrsim 1.5$.

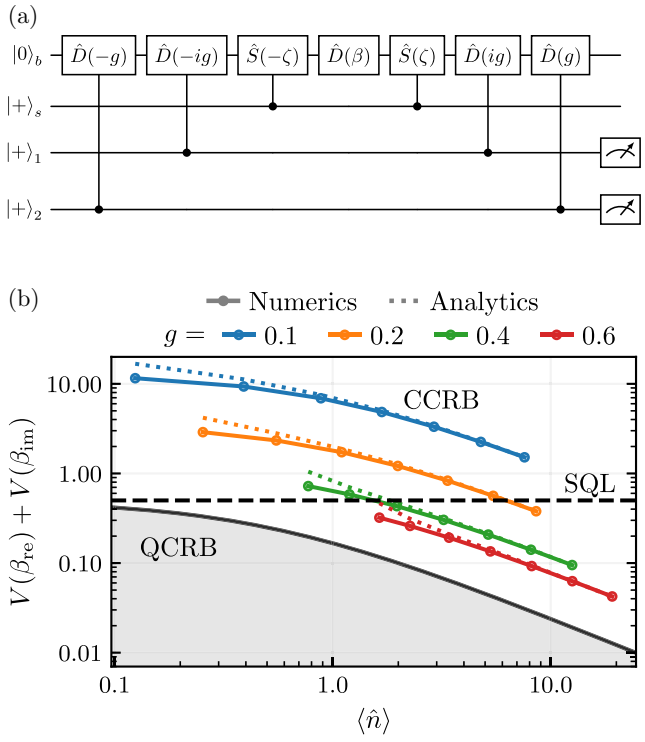



FIG. 3. Joint estimation of the real and imaginary components of a displacement signal using spin-dependent squeezed states. (a) Example measurement protocol for joint-parameter displacement estimation using spin-dependent squeezing, which uses two additional ancillary spins initialized in $|+\rangle_1$ and $|+\rangle_2$, respectively. Spin-dependent displacements conditioned on each ancilla map information about the real and imaginary components of the displacement signal to the ancillas, which are then individually measured. (b) Metrological performance of the measurement scheme for joint displacement parameter estimation. The classical Cramér-Rao bound (colored lines) is shown for $N = 1$ spin at various spin-dependent displacement strengths $g$. For each value of $g$, we vary the squeezing parameter in the range $\zeta \in [0.2, 1.4]$ in steps of 0.2. Solid lines are obtained from numerics, dashed lines are analytics of Eq. (28). The classical Cramér-Rao bound is compared to the standard quantum limit ( dashed black line), defined by the quantum Cramér-Rao bound for bosonic coherent states, $\mathrm{SQL} = 1/2$ [41]. For $g = 0.6$, the classical Cramér-Rao bound is below the standard quantum limit for mode occupations $\langle \hat{n} \rangle \gtrsim 1$. For fixed $\langle \hat{n} \rangle$, the classical Cramér-Rao bound approaches the quantum Cramér-Rao bound (solid black line) as $g$ increases.

## III. ENGINEERING SPIN-DEPENDENT SQUEEZING

In this section we introduce a protocol for the fast preparation of SDS states in many-ion systems. We simultaneously drive the first-order red sideband and blue sideband, each with two tones [see Fig 4(b)]. By stroboscopically varying the phases and detunings of each tone [see Figs. 4(c) and 4(d)], we realize spin-dependent squeezing while minimizing undesired error terms. The duration of our protocol scales favorably as $1/\sqrt{N}$ and can be readily realized on current trapped-ion platforms.

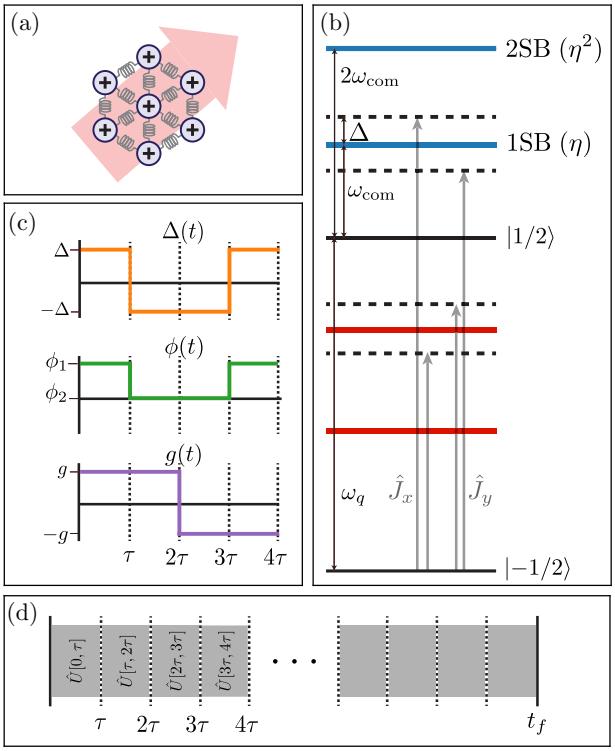



FIG. 4. Experimental protocol for engineering fast and scalable spin-dependent squeezing in a trapped-ion system. (a) We consider a system of $N$ trapped ions coupled via laser interactions to their collective motional mode. (b) Energy diagram for $N = 1$ spin, without loss of generality. Multiple laser tones are tuned close to the first-order sidebands that are $\pm\omega_{\rm COM}$ from the carrier transition $\omega_q$. A first bichromatic field driving interactions in the $\hat{J}_x$ basis is detuned by $\pm(\omega_{\rm COM} + \Delta)$, while a second bichromatic field driving interactions in the $\hat{J}_y$ basis is detuned by $\pm(\omega_{\rm COM} - \Delta)$ (gray lines). The resulting effective spin-dependent squeezing has an interaction strength $\propto \Omega^2\eta^2/\Delta^2$, offering a speedup for appropriately chosen $\Delta$ over alternative approaches that use second-order sideband(2SB) interactions with a weaker coupling strength $\propto \Omega\eta^2$. (c) The laser detuning, phase and interaction strengths are dynamically modulated to obtain the desired spin-dependent squeezing interaction and to minimize unwanted errors from higher-order terms. (d) Schematic of the stroboscopic pulse sequence. Each segment of duration $\tau$ requires evolving under $\hat{H}(t)$ of Eq. (29) with the parameters shown in panel (c). The four segments are repeated $P$ times, with the total protocol duration $t_f$.

### A. Experimental protocol for fast and scalable spin-dependent squeezing

Consider a system of $N$ ions, each with an internal spin-1/2 degree of freedom with transition frequency $\omega_q$, see Fig. 4(a). The combined action of the confining potentials and the Coulomb repulsion supports a set of motional normal modes, which are coupled to the spin degree of freedom via laser-induced interactions. Setting the laser frequency to $\omega_L = \omega_q + \omega_{\rm COM}$ or $\omega_L = \omega_q - \omega_{\rm COM}$ drives the first-order blue sideband or red sideband, respectively, see Fig. 4(b). Here, $\omega_{\rm COM}$ is the frequency of the center-of-mass (COM) mode, which describes uniform excitations of the ions. The strength of the first-order sidebands is linearly proportional to the Lamb-Dicke parameter $\eta = kx_0$, where $k$ is the wave vector and $x_0 = \sqrt{1/(2m\omega)}$ is the harmonic oscillator length scale with $m$ the ion mass, and where we set $\hbar = 1$. Setting $\omega_L = \omega_q + 2\omega_{\rm com}$ or $\omega_L = \omega_q - 2\omega_{\rm com}$ drives the second-order blue or red sideband, respectively, with strength quadratically proportional to the Lamb-Dicke parameter, $\propto \eta^2$.

Spin-dependent squeezing is commonly realized by simultaneously driving the second-order red sideband and blue sidebands [36,37,52]. However, because trapped-ion experiments typically operate in the Lamb-Dicke regime where $\eta \ll 1$, the interaction strength is weak. Here, we realize spin-dependent squeezing with a stronger effective interaction strength by adapting the single-spin protocol of Ref. [45], with experimental demonstrations in Refs. [32,53], to a many-spin system.

Our spin-dependent squeezing protocol is realized by simultaneously driving the first-order sidebands at four different frequencies: one pair of red- and blue-sideband interactions with detuning $\Delta(t)$ and phase of zero, and another pair of red- and blue-sideband interactions with detuning $-\Delta(t)$ and phase $\phi(t)$, see Fig. 4(b). Performing a rotating wave approximation and moving to the interaction picture with respect to the spin and motion, the interaction Hamiltonian is [41]

$$\hat{H}(t) = g(t)\hat{a}\left[\hat{J}_x e^{-it\Delta(t)} + \hat{J}_y e^{it\Delta(t)} e^{-i\phi(t)}\right] + \text{h.c.}, \quad (29)$$

where $g(t) = \eta\Omega(t)/\sqrt{N}$ is the coupling strength between the collective spin and the bosonic mode, and $\Omega(t)$ is the Rabi frequency. To obtain $\hat{H}(t)$, we neglected off-resonant coupling of the sideband interactions to other motional modes, under the assumption that $\Delta(t)$ is small with respect to the frequency spacing between motional modes. Furthermore, we note that time-dependent control over $\Delta(t)$ and $\phi(t)$ has been previously demonstrated in trapped-ion experiments, see, e.g., Refs. 54 and 55. In our

companion work [56], we prove that $H(t)$ provides universal control over the collective spin-boson Hilbert space, which was similarly shown for the single-spin case in Ref. [45].

The real-time dynamics generated by $\hat{H}(t)$ during evolution from $t_0$ to $t$ are described by the Magnus expansion [57],

$$\hat{U}[t_0,t] = \exp\left(-i\hat{\Theta}_1[t_0,t] - \frac{1}{2}\hat{\Theta}_2[t_0,t] + \dots\right), \quad (30)$$

where the first- and second-order terms are, respectively,

$$\hat{\Theta}_1[t_0,t] = \int_{t_0}^{t} dt_1 \hat{H}(t_1), \quad (31a)$$

$$\hat{\Theta}_2[t_0,t] = \int_{t_0}^{t} dt_1 \int_{t_0}^{t_1} dt_2 [\hat{H}(t_1), \hat{H}(t_2)]. \quad (31b)$$

In our protocol, the laser parameters are dynamically modulated to obtain the desired interaction from the Magnus expansion and to minimize unwanted error terms, as discussed below. The parameters $\Delta(t)$, $\phi(t)$ and $g(t)$ are varied according to a stroboscopic sequence consisting of four segments, each of duration $\tau = 2\pi\ell/|\Delta|$ with $\ell \in \mathbb{Z}^+$ an adjustable parameter. The sequence is shown in Fig. 4(c).

During the first segment, the parameters are set to $\Delta(t) = \Delta$, $\phi(t) = \phi_1$ and $g(t) = g$. At the end of this segment, i.e., at $t = \tau$, the first-order Magnus term integrates to zero, $\hat{\Theta}_1[0,\tau] = 0$, because the integral is performed over a complete loop in phase space. The second-order Magnus term is nonzero,

$$\hat{\Theta}_2[0,\tau] = \frac{4\pi g^2 \ell}{\Delta^2}\left[(e^{-i\phi_1}\hat{a}^2 - \text{h.c.})\hat{J}_z - i(\hat{J}_x^2 - \hat{J}_y^2)\right], \quad (32)$$

where the first term is the desired spin-dependent bosonic squeezing. The second term is an unwanted error term that, for $N > 1$, describes rotated two-axis twisting [58,59], and drives transitions between Dicke states. Its dynamics are undone during the second segment, in which $\Delta(t) = -\Delta$ and $\phi(t) = \phi_2$, while $g(t) = g$ is unchanged. At the end of the second segment, i.e., at $t = 2\tau$, the first-order Magnus term again integrates to zero, $\hat{\Theta}_1[\tau,2\tau] = 0$, while the second-order term is

$$\hat{\Theta}_2[\tau,2\tau] = -\frac{4\pi g^2 \ell}{\Delta^2}\left[(e^{-i\phi_2}\hat{a}^2 - \text{h.c.})\hat{J}_z - i(\hat{J}_x^2 - \hat{J}_y^2)\right], \quad (33)$$

which is identical to $\hat{\Theta}_2[0,\tau]$ up to a global sign change and after the replacement $\phi_1 \to \phi_2$. The total evolution after the first and second segments is described by the Baker-Campbell-Hausdorff (BCH) formula,

$$e^{\hat{\Theta}_2[\tau,2\tau]} e^{\hat{\Theta}_2[0,\tau]} = e^{\hat{\Theta}_2[0,\tau] + \hat{\Theta}_2[\tau,2\tau] + \cdots}, \quad (34)$$

from which we see that the phase-independent error-inducing two-axis twisting term always cancels, while the desired spin-dependent squeezing term survives if $\phi_1 \neq \phi_2$.

The third and fourth segments of the stroboscopic sequence are a repetition of the first two segments, but with $g(t) = -g$ [60]. Including these segments results in a many-body echo protocol which, to first order in BCH, cancels all odd-powered Magnus terms. This significantly increases the fidelity of the spin-dependent squeezing, as the leading-order Magnus error term, the third-order term, is canceled.

Both the Magnus expansion and the BCH formula introduce errors originating from higher-order error terms that are not entirely removed by the stroboscopic sequence. We first analyze the remaining leading error terms from the Magnus expansion. For a fixed number of ions $N$, the strength of the $n$th-order Magnus term is $\mathcal{O}(g^n\ell/\Delta^n)$. Scaling $\ell \to \ell\Delta^2/g^2$ ensures that the second-order Magnus term is independent of $g/\Delta$, while in the limit $g/\Delta \to 0$ the higher-order terms are small and can be neglected. Under this scaling of $\ell$, the duration of the segment scales as $\tau \to \tau\Delta/g^2$, which indicates that reducing the strength of the higher-order Magnus terms requires longer segment durations. For nonfixed $N$, the magnitude of higher-order Magnus terms depends on the spin operators that arise from the nested commutators, because their matrix elements depend on $N$. In the Supplemental Material [41], we study the magnitude of the third- and fourth-order Magnus terms with $N$, and show that they are all either bounded above, constant, or decreasing with $N$. Therefore, we expect our protocol to be scalable.

The leading-order BCH error term is, assuming a worst-case scaling of $J_z^2 \propto N^2$, $[\hat{\Theta}_2[0,\tau], \hat{\Theta}_2[\tau,2\tau]] \sim g^4\ell^2N^2/\Delta^4 \sim \eta^4\Omega^4/\Delta^4$. This error is small when $g^2\ell/\Delta^2 \ll 1$, favoring shorter segment durations in the stroboscopic sequence. The amount of spin-dependent squeezing is increased by repeating the full stroboscopic sequence $P$ times. The strength of the $n$th-order Magnus term is then $\mathcal{O}(g^n\ell P/\Delta^n)$, and therefore, to first order in the BCH formula, $P$ plays an identical role to $\ell$ in ensuring that the desired second-order Magnus term is unchanged while $g/\Delta \to 0$ as required to make the higher-order Magnus terms vanish. That is, instead of scaling $\ell \to \ell\Delta^2/g^2$, we have $P \to P\Delta^2/g^2$.

The total duration of the spin-dependent squeezing protocol is calculated from the duration of a single segment, $\tau$, and the number of times $P$ that the four-step stroboscopic

sequence is repeated,

$$t_f = 4P\tau = \frac{8\pi\ell P}{|\Delta|}. \tag{35}$$

In the regime where higher-order Magnus and BCH terms can be neglected, i.e., when $g/\Delta \ll 1$ and $\ell g^2/\Delta^2 \ll 1$, the total evolution is effectively described by the unitary,

$$\hat{S}(\zeta \hat{J}_z) = \exp\left(\frac{1}{2}(\zeta^* \hat{a}^2 - \zeta \hat{a}^{\dagger 2})\hat{J}_z\right), \tag{36}$$

which exactly corresponds to the spin-dependent squeezing operation of Eq. (7) with

$$\zeta = -\frac{8\pi g^2 \ell P(e^{i\phi_1} - e^{i\phi_2})}{\Delta^2}. \tag{37}$$

To maximize the magnitude of the squeezing parameter $|\zeta|$, we set $\phi_2 = \phi_1 - \pi$ which results in $e^{i\phi_1} - e^{i\phi_2} = 2e^{i\phi_1}$. The free parameter $\phi_1$ provides control over the squeezing direction in phase space, while $g$, $\ell$, $P$ and $\Delta$ control both the squeezing amplitude and the relative strength of the higher-order Magnus and BCH terms. A large coupling strength $g$ leads to faster spin-dependent squeezing, but can also require a large detuning $\Delta$ to ensure the higher-order error terms remain small. On the other hand, the number of phase space loops $\ell$ can be kept small, i.e., $\ell = 1$, while $P$ is increased to achieve a larger squeezing magnitude $|\zeta|$.

### B. Speed limit

We investigate the smallest achievable duration required to achieve a target squeezing magnitude in an ideal setting. To do so, we ignore higher-order error terms and consider evolution under the exact spin-dependent squeezing operator of Eq. (36). The duration $t_f$ is minimized when only a single phase loop is performed with $\ell = 1$, and when the stroboscopic sequence is performed only once with $P = 1$, giving $t_f = 4\tau$. Starting from a spin-polarized state, $|-N/2\rangle_s$ or $|N/2\rangle_s$, the bosonic mode is (spin-dependently) squeezed with a squeezing parameter of $z = |\zeta N/2|$. Using Eq. (35) and Eq. (37) with $g = \eta\Omega/\sqrt{N}$, the minimum protocol time $t_f^*$ is

$$t_f^* = \frac{\sqrt{\pi z}}{2g\sqrt{N/2}} = \frac{\sqrt{\pi z}}{\sqrt{2}\eta\Omega}. \tag{38}$$

For a fixed amount of bosonic squeezing $z$, in terms of the Lamb-Dicke parameter $\eta$ and Rabi frequency $\Omega$ the minimum protocol time $t_f^*$ is therefore independent of $N$. In comparison, the duration required to realize spin-dependent squeezing via the second-order sidebands is $t_f^* = 4z/(\eta^2\Omega)$ [36]. When neglecting higher-order terms, our protocol is therefore faster by a factor of $\sqrt{z}/\eta$. Trapped-ion experiments commonly operate in the Lamb-Dicke regime where $\eta \ll 1$, in which our protocol is expected to be significantly faster than using the second-order sidebands. However, higher-order Magnus and BCH terms may prevent the protocol from saturating the speed bound. These terms are negligible only when $g/(\Delta\ell) \ll 1$ and $g^2/\Delta^2 \ll 1$, which requires $t_f \to t_f\,\Delta/g^2$. In the following section, we turn to numerics to further study the protocol's performance, including the impact of higher-order terms.

### C. Numerical results

Here, we numerically study the performance of the protocol in systems of up to $N = 40$ spins using exact numerics. We simulate the dynamics of the Hamiltonian of Eq. (29) using the complete stroboscopic sequence, without any of the approximations used in our analytics [61] The performance is quantified using the fidelity $\mathcal{F} = |\langle\psi_t|\psi(t_f)\rangle|^2$, where $|\psi(t_f)\rangle$ is the final state after the stroboscopic protocol, and $|\psi_t\rangle$ is the ideal target state. The target state is a GHZ spin state that has been subjected to spin-dependent squeezing, $|\psi_t\rangle = \hat{S}(\zeta\hat{J}_z)\,|0\rangle_b\,|\psi_{\mathrm{GHZ}}\rangle_s$, cf. Eq. (10a). The performance of the protocol starting from spin-polarized states, $|0\rangle_b\,|-N/2\rangle_s$, is studied in the Supplemental Material [41].

In Fig. 5(a), we plot the minimum protocol duration $t_{\min}$ (colored lines) required to prepare the target state $|\psi_t\rangle$ with fidelity $\mathcal{F} \geq 0.99$ versus the amount of bosonic squeezing in the target state, $z = |\zeta N/2|$. Because $g$, $\phi_1$, $\ell$ and the target $z$ are fixed, only $P$ and $\Delta$ are left as free parameters in Eq. (37). To minimize $t_{\min}$ for a given target squeezing parameter, we iteratively increase $P$ while obtaining $\Delta$ from Eq. (37) and report the smallest duration for which $\mathcal{F} > 0.99$. This process is repeated for increasing numbers of ions, $N$.

We first compare our protocol against the duration required to realize the same target state using the second-order sidebands (2SB, black dashed line). Overall, we find that the duration using our protocol is significantly smaller than 2SB for all target squeezings. At $z = 1$, the variance of the squeezed quadrature is 8.7 dB below that of a coherent state, calculated using $-10\log_{10}(e^{-2z})$. At this point, we observe an ≈8-fold reduction in protocol duration for $N = 1$, and a ≈15-fold reduction for $N = 10$ and $N = 20$.

We then compare the minimum duration of our protocol with the speed limit $t_f^*$ (gray line) obtained in Eq. (38). For small amounts of squeezing, $z \lesssim 0.5$, we observe that $t_{\min}$ saturates $t_f^*$ for all $N$. In this regime, higher-order Magnus terms are small, permitting $P = 1$ while achieving high fidelities. For moderate amounts of squeezing, $0.5 \lesssim z \lesssim 1.5$, $t_{\min}$ begins to deviate from $t_f^*$, because both $P$ and $\Delta$ increase to ensure the higher-order Magnus terms remain small. The value of $z$ at which $t_{\min}$ departs from $t_f^*$

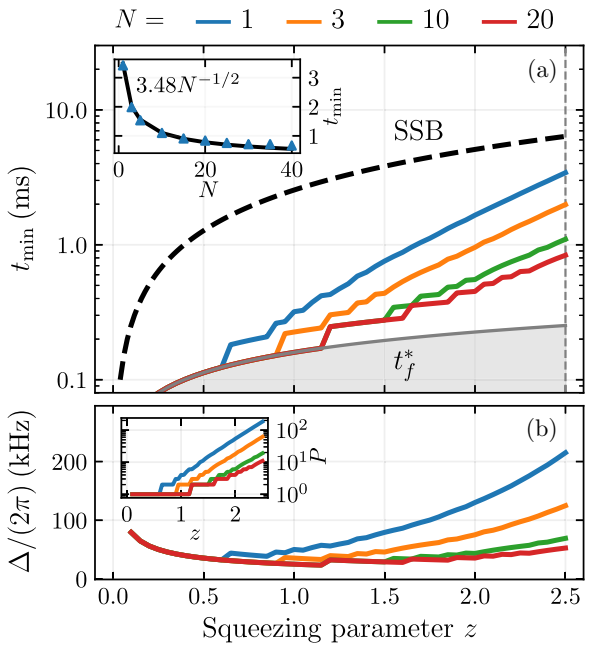



FIG. 5. Performance of first-order sideband protocol to engineer spin-dependent squeezing in a crystal of $N$ ions. (a) Minimum time $t_{\min}$ to prepare a spin-dependent squeezed state $|\psi_t\rangle = \hat{S}(\zeta \hat{J}_z)\,|0\rangle_b\,|\psi_{\mathrm{GHZ}}\rangle_s$ with fidelity $\mathcal{F} > 0.99$ versus squeezing parameter $z = \zeta N/2$. We use a typical coupling strength $g = 2\pi \times 5/\sqrt{N}$ kHz and set the phase-space direction $\phi_1 = \pi$ and the number of phase loops per segment $\ell = 1$. The minimum time is numerically optimized for increasing numbers of ions, $N$, and is compared to the theoretical speed limit $t_f^*$ (gray line). We further compare against the minimum time using second-order sidebands (black dashed line) using $\eta = 0.05$. In the inset, we fix the squeezing to $z = 2.5$ and plot the minimum time $t_{\min}$ for increasing $N$, up to $N = 40$ spins. Solid black line is a least-squares fit to $\propto 1/\sqrt{N}$. (b) Detuning $\Delta$ versus the target squeezing $z$ for increasing number of spins, $N$. The inset plots the number of repetitions, $P$, of the stroboscopic modulation for varying squeezing $z$.

increases with $N$, since the most deleterious higher-order Magnus terms decrease in magnitude with $N$, as we show in the Supplemental Material [41]. The step-like behavior arises from the dependence of $t_f$ on integer values of $P$, with steps becoming indistinguishably small at large $z$.

For large squeezing parameters $z \gtrsim 1.5$, we observe that the protocol duration $t_{\min}$ decreases with $N$. In the inset of Fig. 5(a), we plot $t_{\min}$ with increasing $N$ (triangles) for a fixed squeezing of $z = 2.5$ (21.7 dB). We observe excellent agreement with a least-squares fit (black line) to $1/\sqrt{N}$. The $\sqrt{N}$ reduction in protocol duration is a unique feature of the stroboscopic protocol, and is a clear advantage over the 2SB approach. In the large squeezing regime, we observe an exponential growth of $t_{\min}$ with $z$. Specifically, for $z \gtrsim 2.5$, $t_{\min}$ approaches the 2SB duration, which is particularly prominent for $N = 1$. At extremely large squeezing amplitudes, we expect our protocol to be slower than the 2SB method. However, $z = 2.5$ ($\approx$22 dB of squeezing) is larger than existing experimental demonstrations of motional squeezing in a trapped ion, which typically achieve $\lesssim$20 dB of squeezing [62–64]. Therefore, we do not yet expect this to be a significant limitation of our protocol, and it can be well-mitigated by increasing the number of ions, $N$.

In Fig. 5(b), we plot the detuning $\Delta$ for each point in panel (a), and plot the corresponding number of stroboscopic repetitions $P$ in the inset. For small squeezing parameters $z \lesssim 0.5$, $\Delta$ decreases with $z$ because higher-order Magnus terms are negligible, allowing small values of $P$. We verify in the inset that $P = 1$ for all values of $N$ in this range. In contrast, for $z \gtrsim 0.5$, the higher-order Magnus terms are no longer negligible. Their strength is reduced by increasing $\Delta$ to ensure that the desired second-order term remains significant, which is accompanied by an increase in $P$, again visible in the inset. Although larger $\Delta$ leads to higher theoretical fidelities, in experimental realizations this benefit should be traded off against the fact that larger $\Delta$ leads to both longer protocol times and larger off-resonant coupling to other motional modes. The $\Delta$ required to achieve a target theoretical fidelity at a given $z$ can be lowered by increasing $N$, while off-resonant coupling can be reduced by employing strategies such as optimal control [55,65].

## IV. NOISY DISPLACEMENT SENSING

Realistic quantum sensors are subject to technical noise and decoherence which may degrade their metrological performance. We investigate the impact of decoherence on the displacement sensing performance of reference states obtained from spin-dependent squeezing. We focus on the three decoherence sources that are typically the most deleterious in trapped-ion systems: spin dephasing, motional heating and motional dephasing.

### A. Spin dephasing

We first consider dephasing of the spins, described by $\hat{\sigma}_z$ fluctuations that are identical but independent across all spins. We consider a density matrix, $\rho_s$, that describes a symmetric state of $N$ spins-1/2 in the basis of Dicke states. Single-spin dephasing at a rate $\gamma_s$ for time $t$ causes the $(i,j)$th element of $\rho_s$ to evolve as $\rho_s^{(i,j)}(t) = \rho_s^{(i,j)} \exp(-\gamma_s t |i-j|)$, where $0 \le i,j \le N$. The effect of spin dephasing is most deleterious for GHZ spin states: its density matrix elements $i = 0, j = N$ and $i = N$, $j = 0$ give the maximal scaled dephasing rate, where $|i-j| = N$. Below, we focus on this "worst-case scenario" and investigate the impact of spin dephasing on reference states obtained from applying spin-dependent squeezing to GHZ states.

The evolution of a GHZ spin state $\rho_{\mathrm{GHZ}} = |\psi_{\mathrm{GHZ}}\rangle\langle\psi_{\mathrm{GHZ}}|$ under single-spin dephasing is described by

$$\rho_{\mathrm{GHZ}}(\gamma_s t N) = \frac{1}{2}(|N/2\rangle\langle N/2| + |-N/2\rangle\langle -N/2| + e^{-\gamma_s t N}|N/2\rangle\langle -N/2| + \mathrm{h.c.}). \quad (39)$$

Because spin-dependent squeezing is diagonal in the Dicke basis, the state $\hat{S}(\zeta\hat{J}_z)\rho_{\mathrm{GHZ}}(\gamma t N)\hat{S}^\dagger(\zeta\hat{J}_z)$ exactly describes the application of spin-dependent squeezing, including spin dephasing, to a pure GHZ state for duration $t$. The same state also approximates the state after both noisy GHZ state preparation and noisy spin-dependent squeezing, where $t$ is now the total preparation time.

We assume that the unknown displacement is fast with respect to the decay rate $\gamma_s$, and therefore approximate it as noise-free. After this displacement acts on the reference state, the mixed state encoding $\beta$ is

$$\rho(\beta) = \hat{D}(\beta)\hat{S}(\zeta\hat{J}_z)\rho_{\mathrm{GHZ}}(\gamma_s t N)\hat{S}^\dagger(\zeta\hat{J}_z)\hat{D}^\dagger(\beta). \quad (40)$$

For the mixed state $\rho(\beta)$, the QFI matrix for the estimation of $\boldsymbol{\theta} = \{\beta_{\mathrm{re}}, \beta_{\mathrm{im}}\}$ is (see Supplemental Material for derivation [41]),

$$\boldsymbol{Q}[\rho(\beta)] = (8\langle\hat{n}\rangle + 4)\mathbb{1}. \quad (41)$$

Surprisingly, the QFI matrix identical to the pure state case of Eq. (24), and therefore completely insensitive to spin dephasing. The QFI for the estimation of a displacement amplitude, $Q_{|\beta|}[\rho(\beta)]$ is similarly insensitive to spin dephasing. Displacement sensing with SDS states is therefore robust to spin dephasing. This implies that the metrological utility of SDS states arises due to the mixture of states that are squeezed orthogonally along $\hat{x}$ and $\hat{p}$, not due to the off diagonal coherences.

In contrast, we find that our time-reversal protocol for estimating the displacement's amplitude $|\beta|$, cf. Fig. 1, is sensitive to spin dephasing. The metrological utility is given by the CFI [41],

$$F_{|\beta|}[\rho(\beta)] = \frac{4|\beta|^2 e^{2|\beta|^2}}{e^{2(|\beta|^2\cosh(2z)+\gamma_s t N)} - e^{2|\beta|^2}\cos^2(b)} \times \left[\sinh(2z)\sin(2\phi)\sin(b) + 2\sinh^2(z)\cos(b)\right]^2, \quad (42)$$

where we defined $b = |\beta|^2\sinh(2z)\sin(2\phi)$. First taking the limit of vanishingly small dephasing, $\gamma_s t N \to 0$, and then a vanishingly small displacement amplitude, $|\beta| \to 0$, we recover the pure state result of Eq. (21),

$$\lim_{|\beta|\to 0}\lim_{\gamma_s t N\to 0} F_{|\beta|}[\rho(\beta)] = 4\langle\hat{n}\rangle. \quad (43)$$

In contrast, without first taking the limit of vanishingly small dephasing, the CFI vanishes in the limit of a vanishingly small displacement amplitude only,

$$\lim_{|\beta|\to 0} F_{|\beta|}[\rho(\beta)] = 0. \quad (44)$$

Similar behaviors have previously been observed in time-reversal protocols [15,66]. In our protocol, it arises because spin dephasing results in a degradation in signal contrast which, in the limit $|\beta| \to 0$, implies that changes in the signal due to the displacement cannot be distinguished from changes due to dephasing.

In general, the decay of $F_{|\beta|}[\rho(\beta)]$ with $\exp(\gamma_s t N)$ suggests that the metrological utility of our measurement protocol decreases with increasing $N$. To investigate whether there are parameter regimes where our protocol's metrological utility survives with increasing $N$, we account for the two collective enhancements that arise for realizations in trapped-ion systems. Firstly, an amplification of the displacement amplitude by $|\beta| \to \sqrt{N}|\beta|$. Secondly, using our preparation protocol of Sec. III, the duration to realize spin-dependent squeezing scales as $t \to t/\sqrt{N}$ for a fixed bosonic squeezing parameter $z$. Assuming that the GHZ state preparation time is at most proportional to $\sqrt{N}$ [67], we therefore fix $z$ and scale the spin dephasing exponent as $\gamma_s t N \to \gamma_s t\sqrt{N}$.

In Fig. 6, we plot the CCRB on the estimation variance, $V(|\beta|) \geq 1/F_{|\beta|}[\rho(\beta)]$, as a function of $N$. The variances are obtained using the CFI in the presence of spin dephasing, cf. Eq. (42). In the ideal noise-free case (blue line), the CCRB is only weakly dependent on $N$ and is minimized at $N = 1$. The CCRB grows with $N$ since the displacement amplitude is amplified, moving the CFI away from the optimal point $|\beta| \to 0$. For a given $N$, as $\gamma_s t$ increases we observe that the CCRB grows since dephasing prevents distinguishing of the change in displacement signal from the effects of dephasing. Importantly, for a fixed value of $\gamma_s t$, the CCRB decreases with $N$. This is because the faster preparation time reduces effects from spin dephasing and because the amplified displacement signal can be more easily distinguished from dephasing. The benefit of increasing $N$ is particularly apparent at larger spin dephasing rates: for the largest rate $\gamma_s t = 0.05$, our protocol surpasses the SQL only with $N > 1$. Therefore, provided the displacement amplitudes scales as $|\beta|\sqrt{N}$ and the spin dephasing exponent as $\gamma_s t\sqrt{N}$, there are parameter regimes where the metrological performance of our displacement amplitude sensing scheme improves with increasing numbers $N$ of spins $-1/2$.

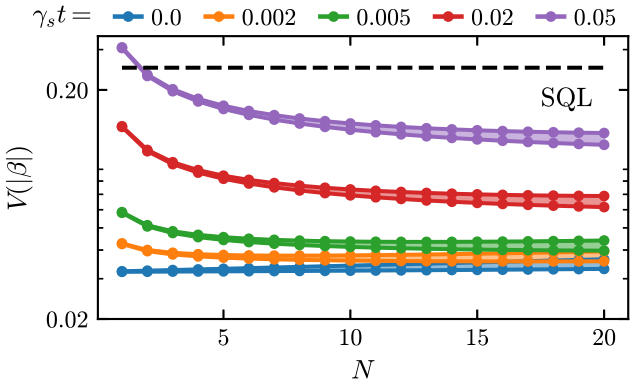



FIG. 6. Classical Cramér-Rao bound for displacement amplitude sensing with spin-dependent squeezed states exposed to spin dephasing. We use the time-reversal protocol of Fig. 2. Here, the displacement amplitude is $|\beta| = 0.02\sqrt{N}$, and the spin-dependent squeezed state amplitude $z = 1.75$. The dephasing exponent is assumed to scale as $\gamma_s t\sqrt{N}$. The dependence on the angle of the displacement, $\phi$, is shown by the shading for each curve. Except for the $N = 1, \gamma_s t = 0.05$ point, the classical Cramér-Rao bound is always below the standard quantum limit (black dashed line). For $\gamma_s t = 0.001$ the classical Cramér-Rao bound is approximately independent of $N$, while for $\gamma_s t = 0.005, 0.02$ and $0.05$ the classical Cramér-Rao bound decays uniformly with $N$.

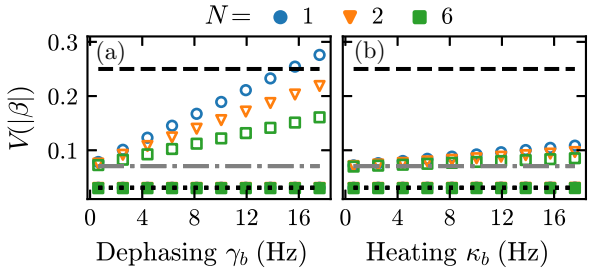



FIG. 7. Metrological performance for displacement amplitude sensing with spin-dependent squeezed states under (a) motional dephasing and (b) motional heating. Metrological utility is measured through quantum (open markers) and classical (closed markers) Cramér-Rao bounds. The bounds are calculated for increasing ion numbers, with $N = 1$ (circles), $N = 2$ (triangles) and $N = 6$ (squares). We also show the standard quantum limit (black dashed line), and noise-free quantum (black dotted line) and classical (gray dash dot line) Cramér-Rao bounds. We set the displacement $\beta = 0.02\sqrt{N}$ and the squeezing parameter $z = 1.5$. The spin-boson coupling strength is $g = 2\pi \times 30/\sqrt{N}$ kHz. Without noise, the spin-dependent squeezed state is prepared by our fast preparation protocol with fidelity $F > 0.99$.

### B. Motional dephasing and heating

Next, we consider sources of motional decoherence by numerically solving the Lindblad master equation,

$$\dot{\rho} = -i[\hat{H}(t), \rho] + \sum_i \gamma_i \left( \hat{L}_i \rho \hat{L}_i - \frac{1}{2}\{\hat{L}_i^\dagger \hat{L}_i, \rho\} \right), \quad (45)$$

where $\hat{L}_i$ is the $i$th jump operator. As in the case of spin dephasing, we focus on motional decoherence occurring during the spin-dependent squeezing operation, and therefore assume that the GHZ state preparation and unknown displacement are noise-free. We realize spin-dependent squeezing using our protocol of Sec. III, which uses the time-dependent spin-boson Hamiltonian of Eq. (29).

We investigate the impact of motional dephasing which, in trapped-ion platforms, models fluctuations of the center-of-mass mode's frequency. The corresponding jump operator is

$$\hat{L}_1 = \hat{n} \quad (46)$$

and occurs at a rate $\gamma_b$. We also consider motional heating, which is typically the most deleterious source of motional decoherence in trapped-ion platforms. Motional heating is described by the two jump operators

$$\hat{L}_1 = \hat{a}, \quad (47a)$$

$$\hat{L}_2 = \hat{a}^\dagger, \quad (47b)$$

both occurring at approximately the same rate, $\kappa_b$.

In Fig 7, we show the metrological utility of reference states obtained from spin-dependent squeezing subject to motional dephasing [panel (a)] and motional heating [panel (b)]. We first observe that the CCRB (open markers) obtained from the time-reversal protocol increases for increasing dephasing and heating rates. We also find that the QCRB (closed markers) minimally increases, although it is not visually apparent within the plotted range, suggesting a strong robustness of the QFI to experimentally relevant decoherence rates.

We also investigate the metrological performance in the presence of motional decoherence for increasing numbers of ions, $N$ (see Fig. 7). For both motional heating and dephasing, we find that the CCRB for a given decay rate decreases with $N$, since the duration of the spin-dependent squeezing protocol decreases as $1/\sqrt{N}$. The Cramér-Rao bound under motional dephasing [panel (a)] is below the SQL for dephasing rates $\gamma_b \lesssim 15$ Hz with $N = 1$. This threshold increases with larger $N$, suggesting a feasible advantage in experiment given achievable parameters. The CCRB under motional heating [panel (b)] is below the SQL for all heating rates considered.

## V. CONCLUSION AND OUTLOOK

We have shown that the QCRB of SDS states saturates the Heisenberg limit for phase-insensitive estimation of

a displacement's magnitude and for simultaneous estimation of a displacement's real and imaginary components. We proposed explicit measurement protocols that follow Heisenberg scaling, which can be readily implemented in current quantum hardware platforms. Moreover, we provided a protocol for preparing SDS states in trapped-ion systems in a fast, scalable manner via dynamically modulated first-order sideband interactions. We showed that the attainable metrological utility is insensitive to spin dephasing and robust to motional heating and motional dephasing. Finally, for our explicit measurement protocols, we demonstrated that even in the presence of decoherence there are regimes where the metrological utility increases with the number of ions, realizing a collective enhancement.

A natural extension of our work would be to develop robust measurement protocols. Moreover, robustness to decoherence occurring during state preparation could potentially be engineered by using quantum control [54,55,64]. More broadly, we expect that our state preparation protocol can be generalized to generate other unitaries such as two-mode squeezing [68] or spin-dependent tri-squeezing [45,53], so as to expand the set of interactions that are available on hybrid many-spin many-boson systems [56].

One could also investigate the metrological performance of reference states prepared with alternative spin-boson entangling unitaries. For example, dispersive interactions have been considered for single-parameter displacement estimation [34,35], but to the best of our knowledge, their suitability for phase-insensitive displacement sensing has not yet been studied.

We also note that there is a wide variety of reference states that have been previously studied for quantum-enhanced displacement sensing. In the Supplemental Material [41], we provide a comparison of our SDS states with other reference states. A detailed comparison of the metrological performance of various reference states in both ideal settings and in the presence of realistic experimental noise would be a valuable analysis that can guide experiments in choosing appropriate protocols tailored to their target hardware.

Looking forward, our phase-insensitive sensing protocol naturally extends to large ion crystals for detecting weak forces or electric fields that induce small displacements. Scaling to $N$ ions both shortens the preparation time of SDS states by $\sqrt{N}$ and amplifies the displacement signal by $\sqrt{N}$. The phase insensitivity is beneficial for dark-matter searches, where the displacement phase is typically unknown, eliminating the need for phase synchronization between the signal and the sensor [6,15]. The same approach applies to quantum-logic-enabled photon-recoil spectroscopy of molecular [69,70] and highly charged ions [71,72], which could benefit atomic clocks [73] and the search for new physics [74].

## ACKNOWLEDGMENTS

We thank Matteo Mazzanti and Rene Gerritsma for insightful discussions. A.S.-N. is supported by the Dutch Research Council (NWO/OCW) as a part of the Quantum Software Consortium (Project No. 024.003.037), QDNL (Project No. NGF.1582.22.030) and ENWXL Grant (Project No. OCENW.XL21.XL21.122). T.R.T. is supported by the Australian Research Council (No. FT220100359) and the U.S. Air Force Office of Scientific Research (No. FA2386-23-1-4062). A.S. acknowledges support by the Department of Science and Technology, Govt. of India, through the INSPIRE Faculty Award (No. DST/INSPIRE/04/2023/001486), by the Anusandhan National Research Foundation (ANRF), Govt. of India, through the Prime Minister's Early Career Research Grant (PMECRG) (No. ANRF/ECRG/2024/001160/PMS) and by IIT Madras through the New Faculty Initiation Grant (NFIG).

## DATA AVAILABILITY

The data that support the findings of this article are openly available [75].

[1] J. Aasi *et al.*, Enhanced sensitivity of the LIGO gravitational wave detector by using squeezed states of light, Nat. Photonics **7**, 613 (2013).

[2] B. P. Abbott *et al.*, (LIGO Scientific Collaboration and Virgo Collaboration), Observation of gravitational waves from a binary black hole merger, Phys. Rev. Lett. **116**, 061102 (2016).

[3] A. Aeppli, K. Kim, W. Warfield, M. S. Safronova, and J. Ye, Clock with $8 \times 10^{-19}$ systematic uncertainty, Phys. Rev. Lett. **133**, 023401 (2024).

[4] A. D. Ludlow, M. M. Boyd, J. Ye, E. Peik, and P. O. Schmidt, Optical atomic clocks, Rev. Mod. Phys. **87**, 637 (2015).

[5] M. S. Turner, Windows on the axion, Phys. Rep. **197**, 67 (1990).

[6] D. Budker, P. W. Graham, H. Ramani, F. Schmidt-Kaler, C. Smorra, and S. Ulmer, Millicharged dark matter detection with ion traps, PRX Quantum **3**, 010330 (2022).

[7] P. Zheng, Y. Cai, B. Xu, S. Wen, L. Zhang, Z. Ni, J. Mai, Y. Zeng, L. Lin, L. Hu, X. Deng, S. Liu, J. Shu, Y. Xu, and D. Yu, Quantum-enhanced dark matter search using cat states, Phys. Rev. Lett. **136**, 171002 (2026).

[8] N. Du *et al.*, (ADMX Collaboration), Search for invisible axion dark matter with the axion dark matter experiment, Phys. Rev. Lett. **120**, 151301 (2018).

[9] C. Braggio, L. Balembois, R. Di Vora, Z. Wang, J. Travesedo, L. Pallegoix, G. Carugno, A. Ortolan, G. Ruoso, U. Gambardella, D. D'Agostino, P. Bertet, and E. Flurin, Quantum-enhanced sensing of axion dark matter with a transmon-based single microwave photon counter, Phys. Rev. X **15**, 021031 (2025).

[10] A. V. Dixit, S. Chakram, K. He, A. Agrawal, R. K. Naik, D. I. Schuster, and A. Chou, Searching for dark matter with a superconducting qubit, Phys. Rev. Lett. **126**, 141302 (2021).
[11] K. M. Backes *et al.*, A quantum enhanced search for dark matter axions, Nature **590**, 238 (2021).
[12] S. Kolkowitz, A. C. Bleszynski Jayich, Q. P. Unterreithmeier, S. D. Bennett, P. Rabl, J. G. E. Harris, and M. D. Lukin, Coherent sensing of a mechanical resonator with a single-spin qubit, Science **335**, 1603 (2012).
[13] S. Schreppler, N. Spethmann, N. Brahms, T. Botter, M. Barrios, and D. M. Stamper-Kurn, Optically measuring force near the standard quantum limit, Science **344**, 1486 (2014).
[14] K. A. Gilmore, J. G. Bohnet, B. C. Sawyer, J. W. Britton, and J. J. Bollinger, Amplitude sensing below the zero-point fluctuations with a two-dimensional trapped-ion mechanical oscillator, Phys. Rev. Lett. **118**, 263602 (2017).
[15] K. A. Gilmore, M. Affolter, R. J. Lewis-Swan, D. Barberena, E. Jordan, A. M. Rey, and J. J. Bollinger, Quantum-enhanced sensing of displacements and electric fields with two-dimensional trapped-ion crystals, Science **373**, 673 (2021).
[16] R. D. Delaney, A. P. Reed, R. W. Andrews, and K. W. Lehnert, Measurement of motion beyond the quantum limit by transient amplification, Phys. Rev. Lett. **123**, 183603 (2019).
[17] C. L. Degen, F. Reinhard, and P. Cappellaro, Quantum sensing, Rev. Mod. Phys. **89**, 035002 (2017).
[18] F. Wolf, C. Shi, J. C. Heip, M. Gessner, L. Pezzè, A. Smerzi, M. Schulte, K. Hammerer, and P. O. Schmidt, Motional Fock states for quantum-enhanced amplitude and phase measurements with trapped ions, Nat. Commun. **10**, 2929 (2019).
[19] X. Deng, S. Li, Z.-J. Chen, Z. Ni, Y. Cai, J. Mai, L. Zhang, P. Zheng, H. Yu, C.-L. Zou, S. Liu, F. Yan, Y. Xu, and D. Yu, Quantum-enhanced metrology with large Fock states, Nat. Phys. **20**, 1874 (2024).
[20] P. T. Grochowski and R. Filip, Optimal phase-insensitive force sensing with non-Gaussian states, Phys. Rev. Lett. **135**, 230802 (2025).
[21] W. Górecki, A. Riccardi, and L. Maccone, Quantum metrology of noisy spreading channels, Phys. Rev. Lett. **129**, 240503 (2022).
[22] W. J. Munro, K. Nemoto, G. J. Milburn, and S. L. Braunstein, Weak-force detection with superposed coherent states, Phys. Rev. A **66**, 023819 (2002).
[23] C. H. Valahu, M. P. Stafford, Z. Huang, V. G. Matsos, M. J. Millican, T. Chalermpusitarak, N. C. Menicucci, J. Combes, B. Q. Baragiola, and T. R. Tan, Quantum-enhanced multiparameter sensing in a single mode, Sci. Adv. **11**, eadw9757 (2025).
[24] K. Duivenvoorden, B. M. Terhal, and D. Weigand, Single-mode displacement sensor, Phys. Rev. A **95**, 012305 (2017).
[25] L. Labarca, S. Turcotte, A. Blais, and B. Royer, Quantum sensing of displacements with stabilized Gottesman-Kitaev-Preskill states, PRX Quantum **7**, 020301 (2026).
[26] F. R. Cardoso, D. Z. Rossatto, G. P. L. M. Fernandes, G. Higgins, and C. J. Villas-Boas, Superposition of two-mode squeezed states for quantum information processing and quantum sensing, Phys. Rev. A **103**, 062405 (2021).
[27] M. G. Genoni, M. G. A. Paris, G. Adesso, H. Nha, P. L. Knight, and M. S. Kim, Optimal estimation of joint parameters in phase space, Phys. Rev. A **87**, 012107 (2013).
[28] Y. Li, X. Cheng, L. Wang, X. Zhao, W. Hou, Y. Li, K. Rehan, M. Zhu, L. Yan, X. Qin, X. Peng, H. Yuan, Y. Lin, and J. Du, Multi-parameter quantum metrology with stabilized multi-mode squeezed state, arXiv:2312.10379.
[29] A. L. Shaw, P. Scholl, R. Finkelstein, R. B.-S. Tsai, J. Choi, and M. Endres, Erasure cooling, control, and hyperentanglement of motion in optical tweezers, Science **388**, 845 (2025).
[30] P. Campagne-Ibarcq, A. Eickbusch, S. Touzard, E. Zalys-Geller, N. E. Frattini, V. V. Sivak, P. Reinhold, S. Puri, S. Shankar, R. J. Schoelkopf, L. Frunzio, M. Mirrahimi, and M. H. Devoret, Quantum error correction of a qubit encoded in grid states of an oscillator, Nature **584**, 368 (2020).
[31] C. Flühmann, T. L. Nguyen, M. Marinelli, V. Negnevitsky, K. Mehta, and J. P. Home, Encoding a qubit in a trapped-ion mechanical oscillator, Nature **566**, 513 (2019).
[32] S. Saner, O. Băzăvan, D. J. Webb, G. Araneda, D. M. Lucas, C. J. Ballance, and R. Srinivas, Generating arbitrary superpositions of nonclassical quantum harmonic oscillator states, arXiv:2409.03482.
[33] M. Penasa, S. Gerlich, T. Rybarczyk, V. Métillon, M. Brune, J. M. Raimond, S. Haroche, L. Davidovich, and I. Dotsenko, Measurement of a microwave field amplitude beyond the standard quantum limit, Phys. Rev. A **94**, 022313 (2016).
[34] R. J. Lewis-Swan, D. Barberena, J. A. Muniz, J. R. K. Cline, D. Young, J. K. Thompson, and A. M. Rey, Protocol for precise field sensing in the optical domain with cold atoms in a cavity, Phys. Rev. Lett. **124**, 193602 (2020).
[35] D. Barberena, R. J. Lewis-Swan, J. K. Thompson, and A. M. Rey, Atom-light entanglement for precise field sensing in the optical domain, Phys. Rev. A **102**, 052615 (2020).
[36] O. Katz, M. Cetina, and C. Monroe, $N$-body interactions between trapped ion qubits via spin-dependent squeezing, Phys. Rev. Lett. **129**, 063603 (2022).
[37] O. Katz, L. Feng, A. Risinger, C. Monroe, and M. Cetina, Demonstration of three- and four-body interactions between trapped-ion spins, Nat. Phys. **19**, 1452 (2023).
[38] Y. Shapira, S. Cohen, N. Akerman, A. Stern, and R. Ozeri, Robust two-qubit gates for trapped ions using spin-dependent squeezing, Phys. Rev. Lett. **130**, 030602 (2023).
[39] M. Ayyash, X. Xu, S. Ashhab, and M. Mariantoni, Driven multiphoton qubit-resonator interactions, Phys. Rev. A **110**, 053711 (2024).
[40] M. K. Hope, J. Lidal, and F. Massel, Preparation of conditionally squeezed states in qubit-oscillator systems, Phys. Rev. Res. **8**, L012046 (2026).
[41] See Supplemental Material at http://link.aps.org/supplemental/10.1103/mhvv-pr5d for (i) a comparison to other reference states, (ii) review of quantum multi-parameter estimation, standard quantum limit and Heisenberg limit, (iii) derivations of the metrological performance of spin-dependent squeezed states, (iv) derivations of the measurement protocols, (v) additional details on the state preparation protocol and (vi) derivations of the metrological performance in the presence of noise, which include Refs. [76–82].

[42] L. Pezzè and A. Smerzi, Advances in multiparameter quantum sensing and metrology, arXiv:2502.17396.
[43] J. Liu, H. Yuan, X.-M. Lu, and X. Wang, Quantum Fisher information matrix and multiparameter estimation, J. Phys. A: Math. Theor. **53**, 023001 (2020).
[44] S. C. Burd, H. M. Knaack, R. Srinivas, C. Arenz, A. L. Collopy, L. J. Stephenson, A. C. Wilson, D. J. Wineland, D. Leibfried, J. J. Bollinger, D. T. C. Allcock, and D. H. Slichter, Experimental speedup of quantum dynamics through squeezing, PRX Quantum **5**, 020314 (2024).
[45] R. T. Sutherland and R. Srinivas, Universal hybrid quantum computing in trapped ions, Phys. Rev. A **104**, 032609 (2021).
[46] M. Ayyash and S. Ashhab, Dispersive regime of multiphoton qubit-oscillator interactions, Phys. Rev. A **112**, 023713 (2025).
[47] Y. Liu, S. Singh, K. C. Smith, E. Crane, J. M. Martyn, A. Eickbusch, A. Schuckert, R. D. Li, J. Sinanan-Singh, M. B. Soley, T. Tsunoda, I. L. Chuang, N. Wiebe, and S. M. Girvin, Hybrid oscillator-qubit quantum processors: Instruction set architectures, abstract machine models, and applications, PRX Quantum **7**, 010201 (2026).
[48] M. Drechsler, M. Belén Farías, N. Freitas, C. T. Schmiegelow, and J. P. Paz, State-dependent motional squeezing of a trapped ion: Proposed method and applications, Phys. Rev. A **101**, 052331 (2020).
[49] N. F. Del Grosso, R. G. Cortiñas, P. I. Villar, F. C. Lombardo, and J. P. Paz, Controlled-squeeze gate in superconducting quantum circuits, Phys. Rev. A **111**, 042606 (2025).
[50] D. M. Greenberger, M. A. Horne, and A. Zeilinger, in *Bell's Theorem, Quantum Theory and Conceptions of the Universe*, edited by M. Kafatos (Springer Netherlands, Dordrecht, 1989), p. 69.
[51] A. Carollo, B. Spagnolo, A. A. Dubkov, and D. Valenti, On quantumness in multi-parameter quantum estimation, J. Stat. Mech. **2019**, 094010 (2019).
[52] D. Wineland, C. Monroe, W. Itano, D. Leibfried, B. King, and D. Meekhof, Experimental issues in coherent quantum-state manipulation of trapped atomic ions, J. Res. Natl. Inst. Stand. Technol. **103**, 259 (1998).
[53] O. Băzăvan, S. Saner, D. J. Webb, E. M. Ainley, P. Drmota, D. P. Nadlinger, G. Araneda, D. M. Lucas, C. J. Ballance, and R. Srinivas, Squeezing, trisqueezing and quadsqueezing in a hybrid oscillator–spin system, Nat. Phys. **22**, 757 (2026).
[54] P. H. Leung, K. A. Landsman, C. Figgatt, N. M. Linke, C. Monroe, and K. R. Brown, Robust 2-qubit gates in a linear ion crystal using a frequency-modulated driving force, Phys. Rev. Lett. **120**, 020501 (2018).
[55] A. R. Milne, C. L. Edmunds, C. Hempel, F. Roy, S. Mavadia, and M. J. Biercuk, Phase-modulated entangling gates robust to static and time-varying errors, Phys. Rev. Appl. **13**, 024022 (2020).
[56] L. J. Bond, C. H. Valahu, T. Tan, and A. Safavi-Naini (to be published).
[57] W. Magnus, On the exponential solution of differential equations for a linear operator, Commun. Pure Appl. Math. **7**, 649 (1954).
[58] J. Ma, X. Wang, C. Sun, and F. Nori, Quantum spin squeezing, Phys. Rep. **509**, 89 (2011).
[59] N. Kotibhaskar, C.-Y. Shih, S. Motlakunta, A. Vogliano, L. Hahn, Y.-T. Chen, and R. Islam, Programmable XY-type couplings through parallel spin-dependent forces on the same trapped ion motional modes, Phys. Rev. Res. **6**, 033038 (2024).
[60] Note that $g(t) \to -g$ can be realized by phase control by sending $\phi_{1,2} \to \phi_{1,2} + \pi$.
[61] The simulations are performed by numerically solving the Schrödinger equation using QuantumOptics.jl [83] in Julia [84] with a Fock space truncation of $n_{\max} = 1660$. This permits us to simulate squeezing amplitudes of up to $|z| \leq 3$ with infidelities due to the truncation of the bosonic Fock space of less than $1 - \mathcal{F} \leq 10^{-4}$. We also simulate the dynamics with $n_{\max} = 1801$ and $n_{\max} = 2000$ to confirm that the finite truncation of bosonic Hilbert space does not impact our results.
[62] D. Kienzler, H.-Y. Lo, B. Keitch, L. de Clercq, F. Leupold, F. Lindenfelser, M. Marinelli, V. Negnevitsky, and J. P. Home, Quantum harmonic oscillator state synthesis by reservoir engineering, Science **347**, 53 (2015).
[63] S. C. Burd, R. Srinivas, J. J. Bollinger, A. C. Wilson, D. J. Wineland, D. Leibfried, D. H. Slichter, and D. T. C. Allcock, Quantum amplification of mechanical oscillator motion, Science **364**, 1163 (2019).
[64] V. G. Matsos, C. H. Valahu, T. Navickas, A. D. Rao, M. J. Millican, X. C. Kolesnikow, M. J. Biercuk, and T. R. Tan, Robust and deterministic preparation of bosonic logical states in a trapped ion, Phys. Rev. Lett. **133**, 050602 (2024).
[65] I. Arrazola, M. B. Plenio, E. Solano, and J. Casanova, Hybrid microwave-radiation patterns for high-fidelity quantum gates with trapped ions, Phys. Rev. Appl. **13**, 024068 (2020).
[66] M. Koppenhöfer and A. A. Clerk, Revisiting the impact of dissipation on time-reversed one-axis-twist quantum-sensing protocols, Phys. Rev. Res. **5**, 043279 (2023).
[67] C. Yin, Fast and accurate Greenberger-Horne-Zeilinger encoding using all-to-all interactions, Phys. Rev. Lett. **134**, 130604 (2025).
[68] M. J. Millican, V. G. Matsos, C. H. Valahu, T. Navickas, L. J. Bond, and T. R. Tan, Engineering continuous-variable entanglement in mechanical oscillators with optimal control, Phys. Rev. Lett. **135**, 233604 (2025).
[69] F. Wolf, Y. Wan, J. C. Heip, F. Gebert, C. Shi, and P. O. Schmidt, Non-destructive state detection for quantum logic spectroscopy of molecular ions, Nature **530**, 457 (2016).
[70] C.-w. Chou, C. Kurz, D. B. Hume, P. N. Plessow, D. R. Leibrandt, and D. Leibfried, Preparation and coherent manipulation of pure quantum states of a single molecular ion, Nature **545**, 203 (2017).
[71] M. G. Kozlov, M. S. Safronova, J. R. Crespo Lopez-Urrutiá, and P. O. Schmidt, Highly charged ions: Optical clocks and applications in fundamental physics, Rev. Mod. Phys. **90**, 045005 (2018).
[72] P. Micke, T. Leopold, S. A. King, E. Benkler, L. J. Spieß, L. Schmöger, M. Schwarz, J. R. Crespo López-Urrutia, and P. O. Schmidt, Coherent laser spectroscopy of highly charged ions using quantum logic, Nature **578**, 60 (2020).
[73] S. A. King, L. J. Spieß, P. Micke, A. Wilzewski, T. Leopold, E. Benkler, R. Lange, N. Huntemann, A. Surzhykov, V. A. Yerokhin, J. R. Crespo López-Urrutia, and P. O. Schmidt,

An optical atomic clock based on a highly charged ion, Nature **611**, 43 (2022).

[74] M. S. Safronova, D. Budker, D. DeMille, D. F. J. Kimball, A. Derevianko, and C. W. Clark, Search for new physics with atoms and molecules, Rev. Mod. Phys. **90**, 025008 (2018).

[75] L.J. Bond, C. Valahu, A. Shankar, T. R. Tan, and A. Safavi Naini, (2026). Data for "Optimal displacement sensing with spin-dependent squeezed states". University of Amsterdam / Amsterdam University of Applied Sciences. Dataset. https://doi.org/10.21942/uva.32270655.v1

[76] Arman and P. K. Panigrahi, Generating overlap between compass states and squeezed, displaced, or Fock states, Phys. Rev. A **109**, 033724 (2024).

[77] G. Bressanini, M. G. Genoni, M. S. Kim, and M. G. A. Paris, Multi-parameter quantum estimation of single- and two-mode pure Gaussian states, Phys. A: Math. Theor. **57**, 315305 (2024).

[78] R. Demkowicz-Dobrzański, W. Górecki, and M. Guţă, Multi-parameter estimation beyond quantum fisher information, J. Phys. A: Math. Theor. **53**, 363001 (2020).

[79] M. Fadel, N. Roux, and M. Gessner, Quantum metrology with a continuous-variable system, Rep. Progr. Phys. **88**, 106001 (2025).

[80] D. Gottesman, A. Kitaev, and J. Preskill, Encoding a qubit in an oscillator, Phys. Rev. A **64**, 012310 (2001).

[81] B. C. Sanders, Superposition of two squeezed vacuum states and interference effects, Phys. Rev. A **39**, 4284 (1989).

[82] F. Toscano, D. A. R. Dalvit, L. Davidovich, and W. H. Zurek, Sub-Planck phase-space structures and Heisenberg-limited measurements, Phys. Rev. A **73**, 023803 (2006).

[83] S. Krämer, D. Plankensteiner, L. Ostermann, and H. Ritsch, Quantumoptics.jl: A Julia framework for simulating open quantum systems, Comput. Phys. Commun. **227**, 109 (2018).

[84] J. Bezanson, A. Edelman, S. Karpinski, and V. B. Shah, Julia: A fresh approach to numerical computing, SIAM Rev. **59**, 65 (2017).